# Low-Strength Type I Interferon Signaling Promotes CAR T-Cell Treatment Efficacy

Erting Tang[1,#], Yifei Hu[1,2,#], Guoshuai Cao[1], Nicholas W. Asby[1], Duy-Thuc Nguyen[1], Nada S. Aboelella[5], Hanna Ruiz[1], Yu Zhao[1], Lishi Xie[3], Xiufen Chen[3], Michael R. Bishop[5,6], Peter A. Riedell[5,6], James L. LaBelle[5], Justin P. Kline[3,4,5,6], Jun Huang[1,3,4,*]

[1]Pritzker School of Molecular Engineering, University of Chicago, Chicago, IL 60637, USA

[2]Pritzker School of Medicine, University of Chicago, Chicago, IL 60637, USA

[3]Committee on Immunology, University of Chicago, Chicago, IL 60637, USA

[4]Committee on Cancer Biology, University of Chicago, Chicago, IL 60637, USA

[5]Section on Hematology/Oncology, Department of Medicine, University of Chicago, Chicago, IL 60637, USA

[6]The David and Etta Jonas Center for Cellular Therapy, University of Chicago, Chicago, IL 60637, USA

[#]These authors contributed equally.

*Correspondence to: huangjun@uchicago.edu

**ABSTRACT**

CD19-directed chimeric antigen receptor (CAR) T-cell therapy has significantly advanced the treatment landscape for relapsed/refractory diffuse large B-cell lymphoma (r/r DLBCL). However, up to 60% of patients do not achieve a complete response. To uncover determinants of therapeutic efficacy, we analyzed the infusion products of eight r/r DLBCL patients with distinct clinical responses to axicabtagene ciloleucel using single-cell transcriptomics. Compared to patients who exhibited progressive disease, infusion products of complete responders demonstrated enriched signatures of type I interferon (IFN-I) signaling. Based on these findings, we developed a novel strategy to improve CD19-directed CAR T-cell treatment efficacy by incorporating IFN-I as an enhancer during the ex vivo manufacturing process. For both CD28- and 4-1BB-costimulated second-generation CARs, we found that low-strength IFN-I signaling enhanced CAR T-cell cytotoxicity and in vivo efficacy. On the other hand, high-strength IFN-I signaling compromised cell viability and in vivo efficacy. Our low-strength IFN-I signaling approach leverages an existing FDA-approved pharmacologic agent and is compatible with current CAR constructs and manufacturing workflows. Together, our results establish IFN-I as a potent and costimulation-independent enhancer of CAR T-cell efficacy and provide a translationally feasible approach to enhance CAR T-cell therapies for r/r DLBCL.

**Key Words:** chimeric antigen receptor (CAR), type I interferon (IFN-I), axicabtagene ciloleucel (axi-cel), lisocabtagene maraleucel (liso-cel), diffuse large B-cell lymphoma (DLBCL)

## INTRODUCTION

Chimeric antigen receptor (CAR) T-cell therapy has advanced the standard-of-care for hematologic malignancies, achieving complete response rates ranging 39-71% across relapsed/refractory diffuse large B-cell lymphoma (r/r DLBCL)[1], acute lymphoblastic leukemia[2], and multiple myeloma[3,4]. However, the therapy's effectiveness is constrained by significant rates of treatment failure. In r/r DLBCL, only ~40% of patients exhibit a complete response, whereas the remaining ~60% of patients exhibit a partial response, stable disease, or progressive disease, as defined by the International Working Group response criteria.[1] Patients who cannot clear their lymphoma burden have limited therapeutic options and often succumb to their disease.

Existing studies have correlated treatment failure with diminished CAR T-cell polyfunctionality[5], increased T-cell exhaustion signatures within CAR T-cell products[6–8], inhibition by CAR Tregs[9], as well as failure of CAR T cells to persist and expand in vivo[1,10], among others[11]. Given the importance of CAR T-cell-intrinsic factors in determining treatment outcomes, we investigated the infusion products (IP) of CAR T-cell therapy patients with r/r DLBCL using single-cell transcriptomics. We observed that, compared to patients with progressive disease, the IPs of complete responders demonstrated enriched signatures of type I interferon (IFN-I) signaling. This observation was also validated using an independent, published dataset from Maus et al.[12]

As potent immunomodulators, IFN-I cytokines have long been of interest for their potential to modulate immunotherapy response rates.[13,14] Upon binding to type I interferon receptors (IFNAR), IFN-I cytokines trigger a phosphorylation cascade that activates transcription factors such as signal transducer and activator of transcription 1 (STAT1), STAT2, and interferon regulatory factor 9 (IRF9).[13] These transcription factors coordinate transcription of interferon-stimulated genes, such as *IRF7*, *MX1*, *ISG15*, *ISG20*, *IFITM1/2/3* which mediate antiviral immunity and effector functions.[13,15] In $CD8^+$ T cells, IFN-I signaling enhances cytotoxicity[16] and induces central memory differentiation[17], while also controlling T-cell exhaustion[18], inhibitory

65 receptor expression[19], and apoptosis[20,21]. Due to their immunomodulatory effects, clinical
66 formulations of IFN-I cytokines (e.g., Avonex, Intron A, Alferon N) have been approved by the
67 FDA for the treatment of malignancies (e.g., hairy cell leukemia, follicular lymphoma)[22],
68 autoimmune diseases (e.g., multiple sclerosis)[23], and viral infections (e.g., hepatitis B and C)[24].
69 Despite being an attractive FDA-approved cytokine for regulating immune functions in cancer,
70 autoimmunity, and infection, IFN-I has not been utilized to modulate CAR T-cell therapy responses.
71 Given our bioinformatic discoveries and the literature-established roles of T-cell-intrinsic
72 IFN-I signaling in modulating T-cell differentiation and functionality[13], we hypothesize that IFN-I
73 signaling enhances CAR T-cell efficacy during the ex vivo manufacturing process. In this study,
74 we detail our discovery and development of IFN-I cytokines as an enhancer to partially address
75 CAR T-cell therapy failure rates. Through in vitro functional assays and in vivo lymphoma
76 xenograft mouse models, we demonstrate proof-of-principle for a novel ex vivo manufacturing
77 method that leverages low-strength, FDA-approved IFN-I cytokines to improve the in vivo
78 treatment efficacy of CAR T-cell therapy.

## RESULTS

*Enrichment of IFN-I signaling in infusion products of complete responders.*

To uncover determinants of therapeutic efficacy, infusion products from 8 r/r DLBCL patients treated with CD28-costimulated CD19-directed CAR T cell therapy (axicabtagene ciloleucel, "axi-cel") at the University of Chicago Medicine were profiled using single-cell sequencing. The cohort included 5 patients who achieved a complete response (CR) at one month post-infusion and another 3 patients who exhibited progressive disease (N-CR) (**Figure 1a**). After removing low-quality cells, we obtained 27,879 cells distributed among 7 T-cell clusters (**Figure 1b**) based on gene expression (**Figure 1c**, figure S1a). No cluster was patient specific (**Figure 1d**, figure S1b). The two CD8$^+$ clusters were annotated as central memory (CM, *SELL*$^+$*IL7R*$^+$*TBX21*$^-$*KLRG1*$^-$) or effector memory (EM, *SELL*$^-$*IL7R*$^+$*TBX21*$^+$*KLRG1*$^+$) T cells. The two CD4$^+$ clusters were annotated as memory (Mem, *FOXP3*$^{lo}$*IL7R*$^+$*CTLA4*$^{lo}$) or regulatory (Treg, *FOXP3*$^{hi}$*IL7R*$^-$*CTLA4*$^{hi}$) T cells. The remaining three clusters consisted of naïve-activated (*SELL*$^+$*IL7R*$^+$*TCF7*$^+$*CD38*$^+$), unconventional (*TRDC*$^+$*NCAM1*$^+$) as a mixture of γδ and natural killer phenotypes, and proliferating (*MKI67*$^+$*TOP2A*$^+$) T cells. No discernable composition differences were found between CR and N-CR patients (**Figure 1b**, **d**, figure S1c).

Gene set enrichment analysis revealed distinct differences between CR and N-CR T cells. CR T cells were enriched for signatures of type I interferon signaling ("IFNα response"), cytolysis, and leukocyte degranulation, whereas N-CR T cells were enriched for signatures of cell growth, hypoxia, and glycolysis (**Figure 1e**). Notably, the CR-specific IFNα response signature was enriched in CR T cells across T-cell clusters (**Figure 1f**) and individual patients (**Figure 1g**).

To validate our discovery of CR-specific IFN-I signaling signatures, we tested our findings using an independent and published single-cell transcriptomic dataset from Maus et al. (*n* = 15 patients with LBCL who received axi-cel, **Figure 1a**).[12] This cohort included 10 patients who

104 achieved a complete response (CR) and 5 who did not (N-CR), as assessed one-month post-
105 infusion. After filtering out low-quality cells, performing dimensionality reduction, and clustering,
106 we uncovered the same 7 T-cell clusters identified in our own dataset (**Figure 1h**) based on gene
107 expression (**Figure 1i**, figure S2a). No cluster was patient specific (**Figure 1j**). Notably, expression
108 of ISGs (including *ISG20*, *IFITM1/3*) was upregulated in IP of CR (figure S2b). Most importantly,
109 IFNα response signatures was enriched in IPs of CR. The CR-specific IFNα response signature
110 was consistently observed across all T-cell clusters except Tregs (**Figure 1k**, figure S2c) and
111 individual patients (**Figure 1l**).
112 Taken together, findings from the discovery and validation datasets strongly support an
113 association between IFN-I signaling and improved CAR T-cell clinical efficacy.
114
115 *IFN-I signaling increases CAR T-cell cytotoxicity.*
116 Previous studies have demonstrated the immunomodulatory role of T cell-intrinsic IFN-I
117 signaling.[13] For instance, IFN-I signaling promotes cytotoxicity[16], $T_h1$ polarization[25–27], and central
118 memory phenotype differentiation[17], all of which may be desired CAR T-cell characteristics and
119 potentially explain the differential clinical responses observed in the two patient cohorts. Based
120 on these findings and our bioinformatics analyses, we hypothesized that IFN-I signaling can
121 enhance CAR T-cell efficacy. To test this hypothesis, we generated both CD28- and 4-1BB-
122 costimulated CD19-directed CAR T cells from primary human T cells. Our CD28-costimulated
123 CAR is based on axicabtagene ciloleucel (axi-cel, **Figure 2b**), whereas our 4-1BB-costimulated
124 is based on lisocabtagene maraleucel (liso-cel, **Figure 2c**). To induce IFN-I signaling, we treated
125 CAR T cells with exogenous IFN-α2, a highly potent, FDA-approved, and clinically compatible
126 IFN-I subtype, for culturing CAR T cells (**Figure 2a**). Prior to addition of IFN-α2, we confirmed that
127 CAR T cells globally expressed the type I interferon receptor in a transduction-independent and
128 costimulation-independent manner (Figure S3a, c).

129 Since each downstream target of IFN-I signaling exhibits varying sensitivity to IFN-I
130 concentrations[28], we hypothesized that the IFN-I culturing concentration may affect CAR T-cell
131 functions. To determine the IFN-I concentrations for our study, we initially titrated IFN-α2 on both
132 CD28- and 4-1BB-costimulated CAR T cells and measured intracellular interferon regulatory
133 factor 7 (IRF7), a key ISG[29] (figure S3b, d). IFN-I signaling reached saturation at concentrations
134 above 3000 IU/mL of IFN-α2, consistent with previous studies.[16,27] We also observed half-maximal
135 IRF7 upregulation at approximately 100-300 IU/mL of IFN-α2. Consequently, we established
136 three culturing conditions: IFN-α2 at saturating concentration ("IFNα-hi", 3000 IU/mL), IFN-α2
137 near half-maximal effective concentration ("IFNα-lo", 300 IU/mL), and no IFN-α2 ("IFNα-neg", 0
138 IU/mL). We confirmed that these conditions resulted in concentration-dependent upregulation of
139 ISGs, including *MX1*, *IRF7*, and *ISG15* (figure S4).
140 CAR T cells were treated based on the three culturing conditions for downstream
141 experimentation (**Figure 2a**). Since IFN-I signaling can inhibit viral transduction[30], we chose to
142 add IFN-α2 after CAR transduction, which enabled us to achieve consistent transduction
143 efficiency and expression of both CD28-costimulated (**Figure 2d**, **f**) and 4-1BB-costimulated
144 CARs (**Figure 2e**, **h**) across the three culturing conditions. Between culturing conditions, IFN-I
145 signaling did not affect CD4/CD8 ratios (**Figure 2g**, **i**), memory phenotypes (figure S5a-d), or IFN-
146 I receptor expression (figure S5e-h). To test cytotoxicity, CAR T cells were co-cultured with OCI-
147 Ly8 target cells, a $CD19^+$ human DLBCL cell line. In both CD28- and 4-1BB-costimulated CAR T
148 cells, we observed IFN-I signaling significantly increased CAR T-cell cytotoxicity (**Figure 2j**, **l**),
149 expression of cytolytic molecules (granzyme B, perforin, **Figure 2k**, **m**), and secretion of cytokines
150 (IL-2, TNF, IFNγ, **Figure 2n-o**), in a concentration-dependent manner. These findings suggest
151 that IFN-I signaling increases CAR T-cell cytotoxicity.
152

153 *High-strength IFN-I signaling increases apoptosis, whereas low-strength IFN-I signaling does not.*
154 After the manufacturing process, both CD28- and 4-1BB-costimulated CAR T cells cultured under
155 the IFNα-hi condition, but not the IFNα-lo condition, consistently yielded fewer viable cells
156 compared to the IFNα-negative condition (**Figure 3a, c**). Given previous reports that IFN-I
157 signaling can inhibit cell proliferation[31], we evaluated whether CAR T-cell proliferation was
158 affected by IFN-I signaling through assessing the proliferation marker, Ki-67. No significant
159 differences in Ki-67 expression were observed across the three culturing conditions, indicating
160 that IFN-I signaling does not impair CAR T-cell proliferation during ex vivo expansion (**Figure 3b,**
161 **d,** figure S6). Since IFN-I signaling also reportedly promotes T-cell apoptosis[20,21], we next
162 quantified CAR T-cell apoptosis via Annexin V staining. Flow phenotyping revealed that CAR T
163 cells in the IFNα-hi condition trended towards increased apoptosis, whereas those in the IFNα-lo
164 condition did not (**Figure 3e-f**).
165 To further investigate the cellularity and apoptosis of CAR T cells from the three culturing
166 conditions following antigen-specific stimulation, we subsequently quantified cellularity and
167 apoptosis of CAR T cells after stimulation with OCI-Ly8 target cells. Following stimulation, CAR
168 T-cell cellularity in the IFNα-lo and IFNα-neg conditions was statistically indistinguishable (**Figure**
169 **3g-h**). On the other hand, CAR T-cell cellularity in the IFNα-hi condition was significantly depleted
170 compared to the other two conditions. At the timepoint when CAR T-cell cellularity in the IFNα-hi
171 condition significantly diverged (day 6 post-stimulation in the representative data), we observed
172 a corresponding enrichment in apoptosis (**Figure 3i-j**).
173 Taken together, these findings suggest that high-strength, but not low-strength IFN-I
174 signaling increases CAR T-cell apoptosis, thereby negatively affecting persistence during both ex
175 vivo expansion and antigen-specific activation.
176

177 *Low-strength IFN-I signaling promotes CAR T-cell treatment efficacy in vivo.*

178 Given that the IFNα-lo condition uniquely increases CAR T-cell functionality (**Figure 2**) without
179 compromising cell viability (**Figure 3**) in both CD28- and 4-1BB-costimulated CAR T cells, our
180 data demonstrate that low-strength IFN-I signaling promotes CAR T-cell efficacy in vitro by
181 balancing function with persistence. Based on these in vitro conclusions, we hypothesized that
182 the IFNα-lo condition uniquely optimizes CAR T-cell treatment efficacy in vivo.

183 To test our hypothesis, we analyzed the efficacy of CAR T cells prepared from the three
184 culturing conditions in a xenograft mouse model based on the OCI-Ly8 cell line (**Figure 4a**). To
185 control for donor-donor heterogeneity, CAR T cells were derived from multiple independent
186 donors (three for CD28-costimulated CAR T cells and two for 4-1BB-costimulated CAR T cells).
187 Across donors, CAR T-cell injection prolonged survival relative to the PBS-only control. For CD28-
188 costimulated CAR T cells with donors 1 and 2, CAR T cells from the IFNα-lo condition significantly
189 prolonged survival and slowed down tumor progression relative to CAR T cells from the IFNα-neg
190 and IFNα-hi conditions (**Figure 4b**, figure S7a). With donor 3, CAR T cells from the IFNα-lo and
191 IFNα-hi conditions performed similarly, but one mouse treated with CAR T cells from IFNα-lo
192 condition demonstrated a notably better and sustained response (figure S7b-c). For 4-1BB-
193 costimulated CAR T cells with donors 4 and 5, CAR T cells from the IFNα-lo condition consistently
194 yielded superior outcomes compared to CAR T cells from the IFNα-neg and IFNα-hi conditions,
195 leading to improved survival and tumor control (**Figure 4c**, figure S7d). Taken together, our
196 findings support our hypothesis and indicate that CAR T cells generated from the IFNα-lo
197 condition, regardless of costimulatory domain, exhibit enhanced in vivo efficacy compared to
198 those from IFNα-neg or IFNα-hi conditions across multiple donors.

199 In conclusion, our in vitro and in vivo studies support a model in which low-strength IFN-I
200 signaling selectively promotes CD28- and 4-1BB-costimulated CAR T-cell treatment efficacy
201 (**Figure 4d**). IFN-I signaling promotes CAR T-cell functionality in a concentration-dependent
202 manner, leading to more effective cytotoxicity, cytokine release, and tumor control. However, at

203 a high enough concentration, IFN-I signaling also increases T-cell apoptosis, leading to reduced
204 yield, poorer persistence, and ineffective tumor control. Although the optimal level of IFN-I
205 signaling may be subject to donor-donor heterogeneity, CAR T cells treated with low-strength
206 IFN-I signaling, regardless of costimulatory domain, consistently exhibit enhanced effector
207 functions without significantly increased apoptosis.

208 **DISCUSSION**

209

210 In this study, we leveraged single-cell transcriptomic analyses of patient IPs from two independent
211 datasets, in vitro functional and phenotypic analyses, and in vivo xenograft mouse studies, to
212 establish that low-strength IFN-I signaling during the ex vivo CAR T-cell manufacturing process
213 selectively promotes CAR T-cell efficacy in vivo in a costimulation-independent manner. Our
214 strategy of harnessing IFN-I signaling to enhance CAR T-cell efficacy is grounded in clinical data
215 and existing literature, while also highlighting IFN-I as an enhancer with significant translational
216 potential for use during the CAR T-cell manufacturing process.

217 There are major attractive qualities that make IFN-I a uniquely promising and translatable
218 enhancer for both CAR T-cell therapy and other emerging cellular therapy modalities. Unlike all
219 other natural and engineered cytokines being developed as CAR T-cell enhancers (including IL-
220 7, IL-10, IL-15, IL-21, Fc-IL-4)[32–36], IFN-Is are uniquely biocompatible drugs with an existing and
221 extensive clinical track record for the treatment of malignancies[22], autoimmune diseases[23], and
222 viral infections[24]. First discovered in the 1950s for their antiviral activities, IFN-I is one of only two
223 cytokines ever approved by the FDA for cancer treatment (the other being IL-2).[37] Biologically,
224 IFN-I elicit a known signaling pathway through the type I interferon receptor to induce antiviral
225 interferon stimulated genes.[13,15] Their pharmacodynamics and pharmacokinetics have been
226 thoroughly explored in pre-clinical and clinical studies.[38] By uniquely employing a biologically,
227 pharmacologically, and clinically characterized pharmacophore, our low-strength IFN-I
228 manufacturing method is straightforward and less likely to introduce uncharacterized toxicities.
229 We also point out that our method was mechanistically inspired by bioinformatics findings from
230 clinical biospecimens, hence we are recapitulating a physiological (rather than a novel) phenotype.

231 In terms of basic biology, our findings are compatible with existing literature on T-cell-
232 intrinsic effects of IFN-I signaling. Enhancement of cytotoxicity and type I cytokine secretion
233 among $CD8^+$ and $CD4^+$ T cells after culturing with exogenous IFN-I is well-established.[16,39]

234 Moreover, the field's current understanding is that T-cell-intrinsic IFN-I signaling leads to different
235 consequences, depending on whether TCR stimulation temporally precedes ("in-sequence") or
236 follows ("out-of-sequence") IFN-I signaling.[13,40] In-sequence signaling generally enhances T-cell
237 functions, while out-of-sequence signaling generally does the opposite.[13] In our studies, since T-
238 cell activation (via CD3/CD28 Dynabeads) preceded IFN-I treatment, our CAR T cells were
239 subject to in-sequence signaling under the current paradigm. Moreover, our findings mirror the
240 expected consequences of in-sequence IFN-I signaling. Lastly, the concentration-dependent
241 nature of our model is compatible with other studies demonstrating that different cellular functions
242 exhibit varying sensitivities to IFN-I signaling.[28]

243 Our findings may also reconcile the currently obscure relationship between IFN-I signaling
244 and CAR T-cell function. On one hand, Jung et al. and Evgin et al. reported that IFN-I signaling
245 hinders CAR T-cell efficacy.[21,41] Both groups subjected their CAR T cells to IFN-β, which has up
246 to 30-fold higher affinity for the type I interferon receptor compared to IFN-α2.[42] Taking into
247 account their high-affinity IFN-I subtype and culturing concentrations, their conditions are similar
248 to our IFNα-hi condition, which accounts for their negative findings. On the other hand, Zhao et
249 al. reported that IFN-I signaling enhances CAR T-cell efficacy.[43] We reason their positive findings
250 are due to their CAR T cells receiving a weak IFN-I stimulus, since they did not add exogenous
251 IFN-I in their in vitro system. In conclusion, our model demonstrates a non-linear relationship
252 between IFN-I signaling and CAR T-cell efficacy, thereby potentially reconciling these intriguing
253 prior studies.

254 There are important limitations to consider from our study. Firstly, our experiments
255 involved CAR T cells generated from healthy donors. However, CAR T cells generated from
256 patients have been subjected to heavy pre-treatment with multiple lines of chemotherapy prior to
257 ex vivo CAR T-cell manufacturing, and may demonstrate increased or decreased responsiveness
258 to IFN-I signaling. Secondly, we test two IFN-I culturing concentrations, but the true optimal
259 concentration may require more granular studies and differ based on donor characteristics. Future

260 studies can examine the biological basis for donor-donor heterogeneity and derive a decision-
261 making algorithm for the best IFN-I dosage. Lastly, although IFN-α2 was specifically chosen for
262 our study, it is unknown whether our model generalizes to the other IFN-I subtypes, many of which
263 exhibit differential biological effects and binding affinities to the IFN-I receptor.[42] These
264 uncharacterized subtypes may represent a wellspring of additional possible cytokine enhancers
265 for the CAR T-cell manufacturing process.

266 **METHODS**

267

268 *Collection of patient biospecimens*

269 Deidentified patient biospecimens were gathered in accordance with ethical guidelines under the
270 institutional review board at the University of Chicago Medicine. Residual infusion product cells
271 were collected from the patient's infusion product bag and stored in CELLBANKER 1 (Amsbio,
272 11888). Cells were cryopreserved in liquid-phase nitrogen.

273

274 *Single-cell RNA-seq data generation.*

275 Cryopreserved biospecimens were thawed and washed with cold FACS buffer (PBS, 2% BSA,
276 0.05% sodium azide). Antibody-stained cells were conjugated with LIVE/DEAD Fixable Near-IR
277 viability dye (Invitrogen, L34975) at 1:1000 dilution in PBS for 5 minutes at room temperature.
278 Finally, cells were washed 3x in cold cell media (RPMI, 10% FBS) before sorting (BD Biosciences,
279 FACSAria Fusion) for live cells. Sorted cells were partitioned into droplets for single-cell RNA-seq
280 via Chromium Next GEM Single-Cell 5'Kit v2 (10x Genomics, 1000263). RNA-seq libraries were
281 prepared according to manufacturer protocols. Libraries were quantified via the Qubit dsDNA HS
282 Assay Kit (Invitrogen, Q32851), quality-checked for fragment sizes via high-sensitivity D5000
283 screentapes (Agilent, 5067-5592), pooled, and sequenced (Illumina, Novaseq-6000 and Nextseq-
284 550).

285

286 *Single-cell RNA-seq data analysis.*

287 Alignment, filtering, counting, and demultiplexing of RNA-seq reads were performed using the
288 Cell Ranger *count* (10x Genomics, version 7.1.0). For alignment, the GRCh38 reference genome
289 was appended with the CAR transgene sequence of axicabtagene ciloleucel.

290 Downstream analysis was performed using Seurat[44] (version 4.3.0). After converting count
291 matrices and merging all Seurat objects, we filtered cells with >15% mitochondrial reads and
292 40,000 UMIs to remove debris, doublets, and dead cells. The matrix was normalized using
293 *NormalizeData* with default options. The top 5,000 variable genes found by *FindVariableFeatures*
294 with the default "vst" method were taken as variable genes. Data were centered and scaled using
295 *ScaleData*, with additional regression against (1) the percent of mitochondrial RNA content and
296 (2) difference in cell cycle S-phase and G2M-phase scores. Scaled data were then used for
297 principal component analysis (PCA) using *RunPCA*. Data harmonization to remove patient-
298 specific effects was performed on the principal components using Harmony[45] (version 0.1.1)
299 through *RunHarmony*. Top 50 harmony components were used for Uniform Manifold and
300 Projection (UMAP) dimensionality reduction via *RunUMAP*. The same harmony components were
301 used to construct the shared nearest neighbor (SNN) graph using *FindNeighbors*, which was then
302 partitioned to identify clusters using *FindClusters* with the "original Louvain" algorithm.
303 Differentially expressed genes were determined using *FindMarkers* in Seurat package
304 with default parameters. Gene set enrichment analysis and pathway enrichment analysis were
305 carried out using clusterProfiler[46] (version 4.6.2) based on pathways from the msigdbr database's
306 built-in msigdbr[47] package (version 7.5.1). Gene module scores were calculated for each cell
307 using *AddModuleScore* in Seurat for msigdbr or customized gene sets.
308
309 *Lentiviral production and transduction.*
310 A GFP-tagged, CD28-costimulated or 4-1BB-costimulated, anti-CD19 human CAR was cloned
311 onto the pHR vector backbone to constitute the transfer plasmid. Plasmids were transfected into
312 the Lenti-X 293T packaging cell line (Takara, 632180) for lentiviral production. In brief, Lenti-X
313 293T cells were seeded and grown overnight to ~90% confluence. Subsequently, transfer,
314 packaging (psPAX2), and envelope (pMD2.G) plasmids were co-transfected into Lenti-X 293T
315 cells via Lipofectamine 3000 (Invitrogen, L3000001). After 72 hours, the viral supernatant was

316 collected and stored at -80°C until transduction. During transduction, lentiviruses were added to
317 human primary T cells along with protamine sulfate (Millipore Sigma, P3369-10G) to a final
318 concentration of 10 µg/mL. Cells were spinoculated at 800 x *g* for 60 minutes at room temperature.
319
320 *CAR T-cell production and culturing.*
321 Cryopreserved human PBMCs were thawed in warm T-cell media (RPMI supplemented with 10%
322 FBS, 1% penicillin/streptomycin, 2 mM L-glutamine, and 50 µM 2-mercaptoethanol).
323 Subsequently, PBMCs were cultured for 3 hours in complete T-cell media (T-cell media
324 supplemented with 50 units/mL of IL-2) in order to allow monocytes to adhere to the culture flask.
325 The non-adhered cells were transferred to a new culture flask. Cells were counted via the LUNA-
326 FL cell counter. T-cell percentage (% $CD3^+$) was calculated by flow cytometry.
327 T cells were seeded in complete T-cell media at 0.75 x $10^6$/mL. CD3/CD28 Dynabeads
328 (Gibco, 11161D) were washed and added at 1:1 ratio. After overnight activation, T cells were
329 transduced with CAR lentiviruses (MOI of 5). The media was refreshed after 24 hours with
330 complete T-cell media dosed with recombinant human IFN-α2 (BioLegend, 592702). T cells were
331 subsequently expanded, and media was refreshed every 2 days.
332
333 *Quantitative reverse transcription PCR.*
334 CAR T cells were treated under IFN-I culturing conditions for 24 hours. Then, cells were collected,
335 and stained for viability (Invitrogen, L34975). Live CAR T cells were sorted (BD Biosciences,
336 FACSAria Fusion). Total RNA was extracted using the Monarch Total RNA Miniprep Kit (NEB,
337 T2010S), according to manufacturer protocols. RNA was quantified via the Qubit RNA HS Assay
338 Kit (Invitrogen, Q32852). cDNA was synthesized using the GoScript Reverse Transcription
339 System (Promega, A5000).
340 Quantitative PCR was performed using Taqman Gene Expression Assay (ThermoFisher
341 Scientifc, 4331182) and Applied Biosystems TaqMan Universal PCR Master Mix (ThermoFisher

342 Scientifc, 4304437), on LightCycler® 96 Instrument (Roche). The cycling conditions were as
343 follows: UNG incubation at 50°C for 2 minutes, initial denaturation at 95°C for 10 minutes, followed
344 by 40 cycles of denaturation at 95°C for 15 seconds and annealing/extension at 60°C for 60
345 seconds. Each sample was run in triplicate.

346 The specific Taqman Gene Expression Assay used were as follows: *ACTB*
347 (Hs01060665_g1), *IRF7* (Hs01014809_g1), *MX1* (Hs00895608_m1), and *ISG15*
348 (Hs01921425_s1). Relative gene expression levels were calculated using the 2^-ΔΔCt method,
349 with *ACTB* serving as the internal control. Statistical analysis was performed using one-way
350 ANOVA followed by a Tukey's post hoc test for significance.

351

352 *In vitro co-culture immunoassays.*

353 For all co-culture immunoassays, CAR T cells (E) and luciferized OCI-Ly8 cells (T) were seeded
354 under a fixed E/T ratio. To measure in vitro cytotoxicity, co-cultures were established with E/T
355 ratio of 1:1. After 6 hours, One-Glo Luciferase substrate (Promega, E6110) was added to each
356 well. Residual tumor cells were quantified via luciferase activity. As a positive control, target cells
357 were directly lysed with 1% NP-40 (Abcam, ab142227). To measure cytotoxic molecule
358 expression, co-cultures were established with E/T ratio of 1:1 with 1x brefeldin A (BioLegend,
359 420601). After 4 hours, cells were collected for intracellular staining and flow cytometry. To
360 measure cytokine secretion, co-cultures were established with E/T ratio of 1:1. After 24 hours, the
361 culture supernatant was collected and stored. Secreted cytokines were quantified using
362 LEGENDplex immunoassays per manufacturer's protocol (BioLegend). To measure in vitro
363 persistence, co-cultures were established with E/T ratio of 1:5. Every three days, cells were
364 counted using Precision Count Beads (BioLegend, 424902) and measured for apoptosis on flow
365 cytometry. Cell media was then refreshed.

366

367 *Flow cytometry.*

368 Cells were washed with cold FACS buffer (PBS, 2% BSA, 0.05% sodium azide). Fc receptors
369 were blocked by incubation with Human TruStain FcX (BioLegend, 422301) at 1:50 dilution for 5
370 minutes at 4°C. Then, cells were incubated for 30 minutes at 4°C in the dark with an antibody
371 staining solution for surface antigen staining . Antibodies were used according to manufacturer
372 recommendations. After staining, cells were incubated briefly either with live/dead staining
373 solution or apoptosis staining solution for 10 minutes at room temperature. Then, cells were either
374 washed and resuspended in FACS buffer or resuspended in Annexin V Binding Buffer (BioLegend,
375 422201). Cells were ready for analysis by flow cytometry or intracellular staining.

376 For intracellular staining, cells stained for surface antigens were subject to the BD
377 Fixation/Permeabilization Kit (BD Biosciences, 554714) for cytotoxic molecule staining or True-
378 Nuclear™ Transcription Factor Buffer Set (BioLegend, 424401) for IRF7 staining, following
379 manufacturer recommendations. In brief, Cells were fixed in fixation buffer, washed 3x in
380 permeabilization buffer, and incubated for 60 minutes at 4°C in the dark with a staining solution
381 containing antibodies and permeabilization buffer. After staining, cells were washed 2x in
382 permeabilization buffer, 1x in FACS buffer, and resuspended in FACS buffer for analysis by flow
383 cytometry.

384 For Ki-67 staining, cells stained for surface antigens were washed 2x in PBS, fixed in
385 prechilled 70% ethanol overnight, washed 2x in FACS buffer, and incubated for 30 minutes at 4°C
386 in the dark with Ki-67 antibody staining solution. After staining, cells were washed 2x in FACS
387 buffer, and resuspended in FACS buffer for analysis by flow cytometry.

388 Flow cytometry was performed on LSRFortessa (BD Biosciences) or Aurora (Cytek
389 Biosciences). Data were analyzed using FlowJo software (version 10.10.0).

390

391 *Antibody panels.*

392 All antibodies were used according to manufacturer recommendations. APC-anti-IFNAR2 (10359-
393 MM07T-A) was from Sino Biological. All other antibodies originate from BioLegend. For surface
394 staining, AF647-anti-CD3 (clone: UCHT1, 300416), BV421-anti-CD3 (clone: UCHT1, 300434),
395 BV510-anti-CD4 (clone SK3, 344633), PerCP/Cy5.5-anti-CD8α (clone SK1, 344709), PE-anti-
396 CD45RA (clone HI100, 304107), BV421-anti-CD45RO (clone UCHL1, 304223), and AF647-anti-
397 CCR7 (clone G043H7, 353217) were used. For intracellular staining, PE/Cy7-anti-granzyme B
398 (clone QA16A02, 372213), PE-anti-perforin (clone B-D48, 353303), and PE-anti-IRF7 (clone
399 12G9A36, 656003) were used. For live/dead staining, Zombie NIR Fixable Viability Kit (423106)
400 was used in PBS. For apoptosis staining, BV421-Annexin V (640923) or PE/Cy7-Annexin V
401 (640950) was diluted in Annexin V Binding Buffer (422201). For Ki-67 staining, PE-anti-Ki-67
402 (clone Ki-67, 350503) was used.

403

404 *Lymphoma xenograft mouse model.*

405 Immunocompromised NOD *scid* IL2Rgamma$^{null}$ (NSG, Strain #005557) mice were purchased
406 from JAX and maintained at the animal resource center (ARC) of the University of Chicago in
407 accordance with institutional guidelines. Mice were monitored daily. Care and experimental
408 procedures were carried out in line with the Institutional Animal Care and Use Committee (IACUC)
409 approved protocols of the Animal Care Center at the University of Chicago.

410 $5\times10^6$ OCI-Ly8-Chili-luc cells in 100 μL PBS were intravenously injected into 8-12-week-
411 old NSG mice to build a xenograft lymphoma model. $5\times10^5$ or $1\times10^6$ CAR T cells were
412 intravenously injected 1 week later. Lymphoma progression was monitored using either IVIS
413 Spectrum (PerkinElmer) or Lago X (Spectral Instruments Imaging) following the Intraperitoneal
414 injection of D-luciferin potassium (PerkinElmer, 122799). Animals were anesthetized at 2%
415 isoflurane throughout acquisition. Bioluminescence was quantified with Aura software (Spectral

416 Instruments Imaging). Mice were euthanized upon manifestation of paralysis, impaired mobility,
417 or poor body condition (BCS<2).
418
419 *Statistical analysis.*
420 Statistical tests were performed on R (version 4.2.1) or GraphPad Prism 10 (version 10.1.1).
421 Comparisons between two groups were performed using Wilcoxon Rank-Sum test. Comparisons
422 between more than two groups were performed by either one-way or two-way ANOVA followed
423 by Tukey correction for multiple comparisons. Survival data were analyzed using the Log-Rank
424 (Mantel-Cox) test. To assess correlation, Spearman's rank correlation coefficient was calculated,
425 as indicated.
426
427 *Data availability.*
428 All data are available from the authors upon reasonable request.
429
430 *Code availability.*
431 Codes supporting the analyses performed in this study are available at
432 https://github.com/ertingtang/IFN-I-CART.

433 **ACKNOWLEDGEMENTS**

434

435 We thank the NIH New Innovator award (1DP2AI144245) and NIH R21AI169159 for financial
436 support (to J.H.). Y.H. was supported by the University of Chicago MSTP Training Grant
437 (T32GM007281). N.W.A. was supported by the University of Chicago MTCR training grant
438 (T32CA009594). Flow cytometry was performed at the Cytometry and Antibody Technology
439 Facility at University of Chicago, which receives financial support from the Cancer Center Support
440 Grant (P30CA014599). Live bioluminescence imaging was performed at the University of Chicago
441 Integrated Small Animal Imaging Research Resource. We thank the UChicago Blood Donation
442 Center for healthy donor PBMCs. We thank Aniruddhsingh Solanki at the animal resource center
443 at University of Chicago for excellent technical assistance.

## AUTHOR CONTRIBUTIONS

Y.H. and E.T. designed the study, designed experiments, analyzed and interpreted data and wrote the manuscript. J.H. supervised the project and edited the manuscript. E.T., G.C., Y.Z. performed single-cell analyses. Y.H., generated single-cell patient data. Y.H., E.T., and N.W.A. performed in vitro experimentation. E.T., D.N., N.S.A, and Y.H. performed in vivo studies. P.A.R. coordinated patient biospecimens for these studies. All authors contributed intellectually or assisted with experiments in this manuscript.

452 **DECLARATIONS OF INTERESTS**

453

454 J.H., Y.H., and E.T. are listed as inventors on a patent related to interferon-enhanced CAR-T cells
455 (US provisional patent application 63/789,043). J.L.L. reports other grants from AbbVie and the
456 American Cancer Society outside the submitted work. No disclosures were reported by the other
457 authors. P.A.R. reports Research Support/Funding: BMS, Kite Pharma, Inc./Gilead, MorphoSys,
458 Calibr, Tessa Therapeutics, Fate Therapeutics, Xencor, and Novartis Pharmaceuticals
459 Corporation. Speaker's Bureau: Kite Pharma, Inc./Gilead; Consultancy on advisory boards:
460 AbbVie, Novartis Pharmaceuticals Corporation, BMS, Janssen, BeiGene, Karyopharm
461 Therapeutics Inc., Takeda Pharmaceutical Company, Kite Pharma, Inc./Gilead, Sana
462 Biotechnology, Nektar Therapeutics, Nurix Therapeutics, Intellia Therapeutics, and Bayer.
463 Honoraria: Novartis Pharmaceuticals Corporation. M.R.B. reports Membership on an Advisory
464 Board or Consultancy for Kite/Gilead, Novartis, CRISPR Therapeutics, Autolus Therapeutics,
465 BMS, Incyte, Sana Biotechnology, Iovance Biotherapeutics. He has served on a Speakers Bureau
466 for BMS, Kite/Gilead, Agios, and Incyte. J.P.K. receives research support from Merck, Verastem,
467 and iTeos; has served on a speaker's bureau for Kite/Gilead; and has served on advisory boards
468 for Verastem, Seattle Genetics, MorphoSys, and Karyopharm.

469 **REFERENCES**

470


471 1. Neelapu, S. S. *et al.* Axicabtagene Ciloleucel CAR T-Cell Therapy in Refractory Large B-
472 Cell Lymphoma. *N. Engl. J. Med.* **377**, 2531–2544 (2017).
473 2. Maude, S. L. *et al.* Tisagenlecleucel in Children and Young Adults with B-Cell
474 Lymphoblastic Leukemia. *N. Engl. J. Med.* **378**, 439–448 (2018).
475 3. Rodriguez-Otero, P. *et al.* Ide-cel or Standard Regimens in Relapsed and Refractory
476 Multiple Myeloma. *N. Engl. J. Med.* **388**, 1002–1014 (2023).
477 4. San-Miguel, J. *et al.* Cilta-cel or Standard Care in Lenalidomide-Refractory Multiple
478 Myeloma. *N. Engl. J. Med.* **389**, 335–347 (2023).
479 5. Rossi, J. *et al.* Preinfusion polyfunctional anti-CD19 chimeric antigen receptor T cells are
480 associated with clinical outcomes in NHL. *Blood* **132**, 804–814 (2018).
481 6. Fraietta, J. A. *et al.* Determinants of response and resistance to CD19 chimeric antigen
482 receptor (CAR) T cell therapy of chronic lymphocytic leukemia. *Nat. Med.* **24**, 563–571
483 (2018).
484 7. Deng, Q. *et al.* Characteristics of anti-CD19 CAR T cell infusion products associated with
485 efficacy and toxicity in patients with large B cell lymphomas. *Nat. Med.* **26**, 1878–1887
486 (2020).
487 8. Finney, O. C. *et al.* CD19 CAR T cell product and disease attributes predict leukemia
488 remission durability. *J. Clin. Invest.* **129**, 2123–2132 (2019).
489 9. Good, Z. *et al.* Post-infusion CAR TReg cells identify patients resistant to CD19-CAR
490 therapy. *Nat. Med.* **28**, 1860–1871 (2022).
491 10. Schuster, S. J. *et al.* Tisagenlecleucel in adult relapsed or refractory diffuse large B-cell
492 lymphoma. *N. Engl. J. Med.* **380**, 45–56 (2019).
493 11. Cheng, J. *et al.* Understanding the Mechanisms of Resistance to CAR T-Cell Therapy in
494 Malignancies. *Frontiers in Oncology* vol. 9 1237 at

495 https://doi.org/10.3389/fonc.2019.01237 (2019).
496 12. Haradhvala, N. J. *et al.* Distinct cellular dynamics associated with response to CAR-T
497 therapy for refractory B cell lymphoma. *Nat. Med.* **28**, 1848–1859 (2022).
498 13. Crouse, J., Kalinke, U. & Oxenius, A. Regulation of antiviral T cell responses by type I
499 interferons. *Nature Reviews Immunology* vol. 15 231–242 at
500 https://doi.org/10.1038/nri3806 (2015).
501 14. Musella, M., Manic, G., De Maria, R., Vitale, I. & Sistigu, A. Type-I-interferons in infection
502 and cancer: Unanticipated dynamics with therapeutic implications. *Oncoimmunology* **6**,
503 1–12 (2017).
504 15. Ning, S., Pagano, J. S. & Barber, G. N. IRF7: Activation, regulation, modification and
505 function. *Genes and Immunity* vol. 12 399–414 at https://doi.org/10.1038/gene.2011.21
506 (2011).
507 16. Curtsinger, J. M., Valenzuela, J. O., Agarwal, P., Lins, D. & Mescher, M. F. Cutting Edge:
508 Type I IFNs Provide a Third Signal to CD8 T Cells to Stimulate Clonal Expansion and
509 Differentiation. *J. Immunol.* **174**, 4465–4469 (2005).
510 17. Ramos, H. J. *et al.* Reciprocal responsiveness to interleukin-12 and interferon-α specifies
511 human CD8+ effector versus central memory T-cell fates. *Blood* **113**, 5516–5525 (2009).
512 18. Lukhele, S. *et al.* The transcription factor IRF2 drives interferon-mediated CD8+ T cell
513 exhaustion to restrict anti-tumor immunity. *Immunity* **55**, 2369-2385.e10 (2022).
514 19. Sumida, T. S. *et al.* Type I interferon transcriptional network regulates expression of
515 coinhibitory receptors in human T cells. *Nat. Immunol.* **23**, 632–642 (2022).
516 20. Harrer, D. C. *et al.* CAR Triggered Release of Type-1 Interferon Limits CAR T-Cell
517 Activities by an Artificial Negative Autocrine Loop. *Cells* **11**, (2022).
518 21. Evgin, L. *et al.* Oncolytic virus-derived type I interferon restricts CAR T cell therapy. *Nat.*
519 *Commun.* **11**, 1–15 (2020).
520 22. Musella, M., Manic, G., De Maria, R., Vitale, I. & Sistigu, A. Type-I-interferons in infection

521 and cancer: Unanticipated dynamics with therapeutic implications. *Oncoimmunology* **6**,
522 1–12 (2017).
523 23. Jakimovski, D., Kolb, C., Ramanathan, M., Zivadinov, R. & Weinstock-Guttman, B.
524 Interferon β for Multiple Sclerosis. *Cold Spring Harb. Perspect. Med.* **8**, 1–19 (2018).
525 24. Li, S. F. *et al.* Type i interferons: Distinct biological activities and current applications for
526 viral infection. *Cellular Physiology and Biochemistry* vol. 51 2377–2396 at
527 https://doi.org/10.1159/000495897 (2018).
528 25. Cho, S. S. *et al.* Activation of STAT4 by IL-12 and IFN-alpha: evidence for the
529 involvement of ligand-induced tyrosine and serine phosphorylation. *J. Immunol.* **157**,
530 (1996).
531 26. Huber, J. P., Ramos, H. J., Gill, M. A. & Farrar, J. D. Cutting Edge: Type I IFN Reverses
532 Human Th2 Commitment and Stability by Suppressing GATA3. *J. Immunol.* **185**, 813–
533 817 (2010).
534 27. Ramgolam, V. S., Sha, Y., Jin, J., Zhang, X. & Markovic-Plese, S. IFN-β Inhibits Human
535 Th17 Cell Differentiation. *J. Immunol.* **183**, 5418–5427 (2009).
536 28. Mendoza, J. L. *et al.* The IFN-λ-IFN-λR1-IL-10Rβ Complex Reveals Structural Features
537 Underlying Type III IFN Functional Plasticity. *Immunity* **46**, 379–392 (2017).
538 29. Marie, I., Durbin, J. & Levy, D. Differential viral induction of distinct interferon-alpha genes
539 by positive feedback through interferon regulatory factor-7. *EMBO J.* **17**, 6660–6669
540 (1998).
541 30. Durgin, J., Sannecy, A., Kelly, A., O'Connor, R. S. & Ghassemi, S. Type I Interferon
542 Blockade Enhances Transduction Efficiency and Efficacy of Non-Activated CAR T Cells.
543 *Blood* **142**, 6830–6830 (2023).
544 31. Cheon, H. J., Wang, Y., Wightman, S. M., Jackson, M. W. & Stark, G. R. How cancer
545 cells make and respond to interferon-I. *Trends in Cancer* **9**, 83–92 (2023).
546 32. Alizadeh, D. *et al.* IL15 enhances CAR-T cell antitumor activity by reducing mTORC1

547 activity and preserving their stem cell memory phenotype. *Cancer Immunol. Res.* **7**, 759–
548 772 (2019).
549 33. Li, L. *et al.* Transgenic expression of IL-7 regulates CAR-T cell metabolism and enhances
550 in vivo persistence against tumor cells. *Sci. Rep.* **12**, 1–14 (2022).
551 34. Štach, M. *et al.* Inducible secretion of IL-21 augments anti-tumor activity of piggyBac-
552 manufactured chimeric antigen receptor T cells. *Cytotherapy* **22**, 744–754 (2020).
553 35. Zhao, Y. *et al.* IL-10-expressing CAR T cells resist dysfunction and mediate durable
554 clearance of solid tumors and metastases. *Nat. Biotechnol.* (2024) doi:10.1038/s41587-
555 023-02060-8.
556 36. Feng, B. *et al.* The type 2 cytokine Fc–IL-4 revitalizes exhausted CD8+ T cells against
557 cancer. *Nature* **634**, (2024).
558 37. Berraondo, P. *et al.* Cytokines in clinical cancer immunotherapy. *Br. J. Cancer* **120**, 6–15
559 (2019).
560 38. Buchwalder, P., Buclin, T., Trinchard, I., Munafo, A. & Biollaz, J. Pharmacokinetics and
561 Pharmacodynamics of IFN-b1a in Healthy Volunteers. *J. Interf. Cytokine Res.* **20**, 857–
562 866 (2000).
563 39. Davis, A. M., Ramos, H. J., Davis, L. S. & Farrar, J. D. Cutting Edge: A T-bet-
564 Independent Role for IFN-α/β in Regulating IL-2 Secretion in Human CD4 + Central
565 Memory T Cells. *J. Immunol.* **181**, 8204–8208 (2008).
566 40. van Boxel-Dezaire, A. H. H., Rani, M. R. S. & Stark, G. R. Complex Modulation of Cell
567 Type-Specific Signaling in Response to Type I Interferons. *Immunity* **25**, 361–372 (2006).
568 41. Jung, I. Y. *et al.* Type I Interferon Signaling via the EGR2 Transcriptional Regulator
569 Potentiates CAR T Cell–Intrinsic Dysfunction. *Cancer Discov.* **13**, 1636–1655 (2023).
570 42. Ng, C. T., Mendoza, J. L., Garcia, K. C. & Oldstone, M. B. A. Alpha and Beta Type 1
571 Interferon Signaling: Passage for Diverse Biologic Outcomes. *Cell* **164**, 349–352 (2016).
572 43. Zhao, Z. *et al.* Structural Design of Engineered Costimulation Determines Tumor

573 Rejection Kinetics and Persistence of CAR T Cells. *Cancer Cell* **28**, 415–428 (2015).
574 44. Hao, Y. *et al.* Integrated analysis of multimodal single-cell data. *Cell* **184**, 3573-3587.e29
575 (2021).
576 45. Korsunsky, I. *et al.* Fast, sensitive and accurate integration of single-cell data with
577 Harmony. *Nat. Methods* **16**, 1289–1296 (2019).
578 46. Wu, T. *et al.* clusterProfiler 4.0: A universal enrichment tool for interpreting omics data.
579 *Innovation* **2**, (2021).
580 47. Subramanian, A. *et al.* Gene set enrichment analysis: A knowledge-based approach for
581 interpreting genome-wide expression profiles. *Proc. Natl. Acad. Sci. U. S. A.* **102**, 15545–
582 15550 (2005).
583 48. Cao, G. *et al.* Two-stage CD8 + CAR T-cell differentiation in patients with large B-cell
584 lymphoma. *Nat. Commun.* (2025) doi:10.1038/s41467-025-59298-w.
585

## MAIN FIGURES AND LEGENDS

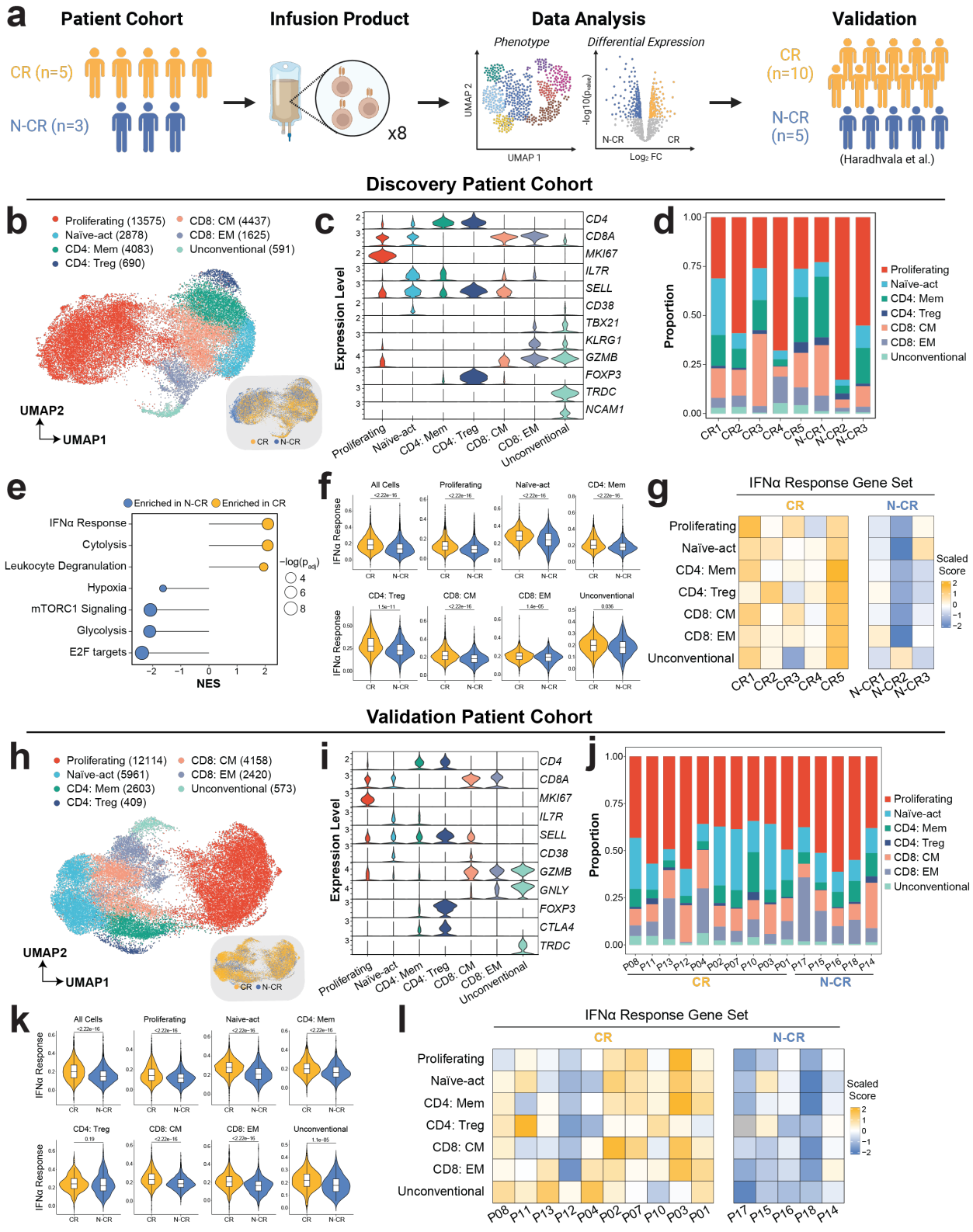


587

**Figure 1. Enrichment of IFN-I signaling in infusion products of complete responders.** (**a**) Cartoon depicting study design of single-cell analysis on infusion products of patients who received axi-cel from discovery dataset and validation datasets. CR, complete responder, N-CR, non-complete responder. (**b**) UMAP demonstrating 7 T-cell clusters in infusion product from discovery dataset. (**c**) Violin plots depicting normalized expression levels of representative markers for each cluster. (**d**) Stacked bar graphs depicting T-cell cluster proportions for each patient in discovery dataset. (**e**) Gene set enrichment analysis comparing CR and N-CR T cells. For each gene set, direction and statistical significance of enrichment are indicated by the circle's color and size, respectively. (**f**) Violin plots depicting IFNα response signature scores in CR and N-CR T cells from each T-cell cluster. Signature scores were compared by Wilcoxon Rank-Sum test. (**g**) Tilemap depicting scaled IFNα response signature scores in each T-cell cluster across patients. (**h**) UMAP demonstrating 7 T-cell clusters in infusion product from validation dataset from Maus et al. (**i**) Violin plots depicting normalized expression levels of representative markers for each cluster. (**j**) Stacked bar graphs depicting T-cell cluster proportions for each patient in validation dataset. (**k**) Violin plots depicting signature scores in CR and N-CR T cells from each T-cell cluster. Signature scores were compared by Wilcoxon Rank-Sum test. (**l**) Tilemap depicting scaled signature scores of IFNα response gene sets in each T-cell cluster across patients. No Treg was found in P17 infusion products, colored in gray.

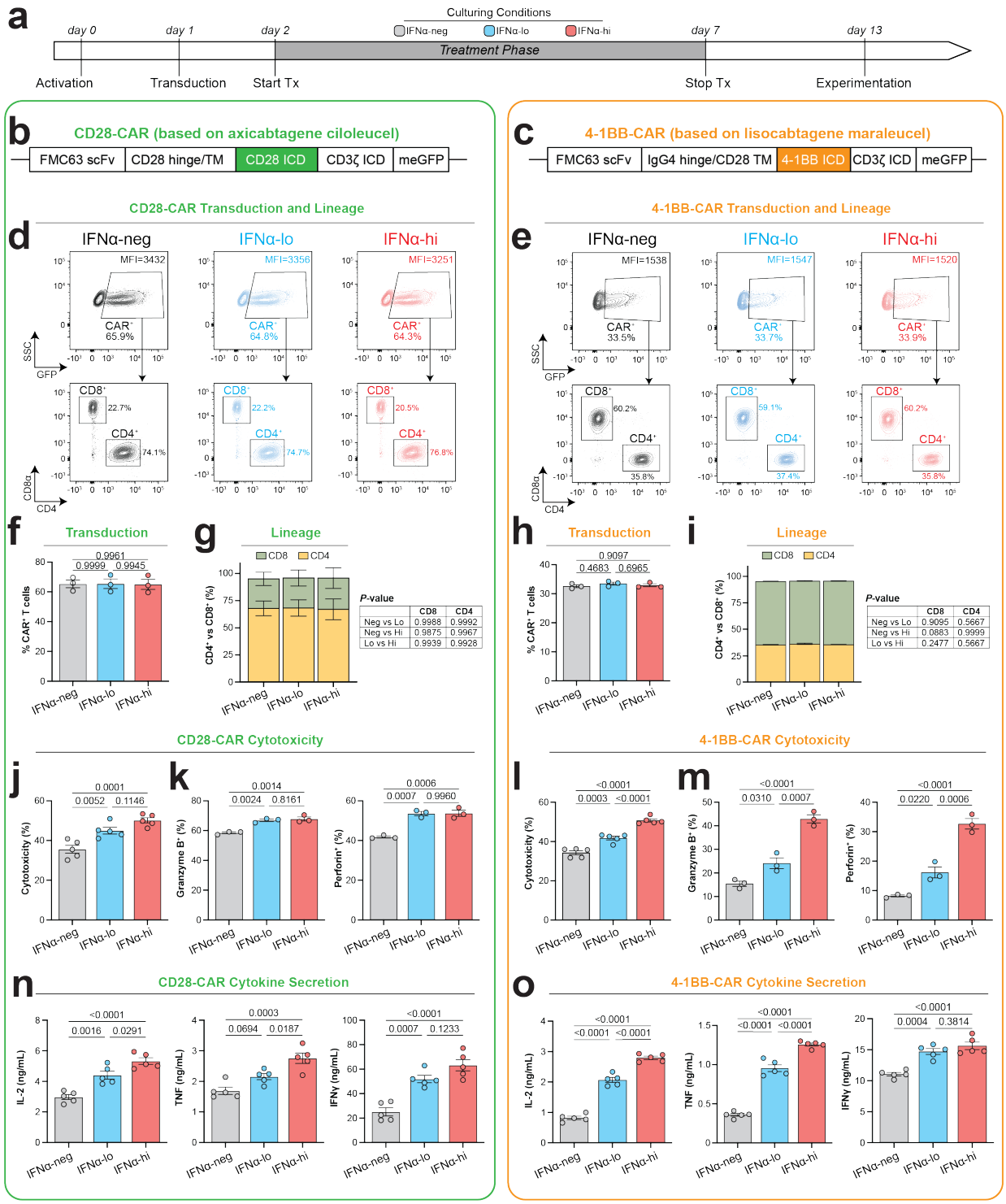
a
Culturing Conditions
IFNα-neg
IFNα-lo
IFNα-hi
day 0
day 1
day 2
day 7
day 13
Treatment Phase
Activation
Transduction
Start Tx
Stop Tx
Experimentation
b
CD28-CAR (based on axicabtagene ciloleucel)
FMC63 scFv
CD28 hinge/TM
CD28 ICD
CD3ζ ICD
meGFP
c
4-1BB-CAR (based on lisocabtagene maraleucel)
FMC63 scFv
IgG4 hinge/CD28 TM
4-1BB ICD
CD3ζ ICD
meGFP
CD28-CAR Transduction and Lineage
4-1BB-CAR Transduction and Lineage
d
e
IFNα-neg
IFNα-lo
IFNα-hi
MFI=3432
MFI=3356
MFI=3251
MFI=1538
MFI=1547
MFI=1520
CAR+ 65.9%
CAR+ 64.8%
CAR+ 64.3%
CAR+ 33.5%
CAR+ 33.7%
CAR+ 33.9%
SSC
GFP
CD8+ 22.7%
CD4+ 74.1%
CD8+ 22.2%
CD4+ 74.7%
CD8+ 20.5%
CD4+ 76.8%
CD8+ 60.2%
CD4+ 35.8%
CD8+ 59.1%
CD4+ 37.4%
CD8+ 60.2%
CD4+ 35.8%
CD8α
CD4
f
Transduction
% CAR+ T cells
0.9961
0.9999
0.9945
IFNα-neg
IFNα-lo
IFNα-hi
g
Lineage
CD8
CD4
CD4+ vs CD8+ (%)
P-value
CD8 CD4
Neg vs Lo 0.9988 0.9992
Neg vs Hi 0.9875 0.9967
Lo vs Hi 0.9939 0.9928
h
Transduction
% CAR+ T cells
0.9097
0.4683
0.6965
i
Lineage
CD4+ vs CD8+ (%)
P-value
CD8 CD4
Neg vs Lo 0.9095 0.5667
Neg vs Hi 0.0883 0.9999
Lo vs Hi 0.2477 0.5667
CD28-CAR Cytotoxicity
4-1BB-CAR Cytotoxicity
j
Cytotoxicity (%)
0.0001
0.0052
0.1146
k
Granzyme B+ (%)
0.0014
0.0024
0.8161
Perforin+ (%)
0.0006
0.0007
0.9960
l
Cytotoxicity (%)
<0.0001
0.0003
<0.0001
m
Granzyme B+ (%)
<0.0001
0.0310
0.0007
Perforin+ (%)
<0.0001
0.0220
0.0006
n
CD28-CAR Cytokine Secretion
IL-2 (ng/mL)
<0.0001
0.0016
0.0291
TNF (ng/mL)
0.0003
0.0694
0.0187
IFNγ (ng/mL)
<0.0001
0.0007
0.1233
o
4-1BB-CAR Cytokine Secretion
IL-2 (ng/mL)
<0.0001
<0.0001
<0.0001
TNF (ng/mL)
<0.0001
<0.0001
<0.0001
IFNγ (ng/mL)
<0.0001
0.0004
0.3814
IFNα-neg
IFNα-lo
IFNα-hi

606

607 **Figure 2. IFN-I signaling increases CAR T-cell cytotoxicity.**
608 (**a**) Workflow of CAR T-cell ex vivo generation, treatment, and culturing. (**b**-**c**) CD28- or 4-1BB-
609 costimulated CAR designs based on the construct used in axicabtagene ciloleucel (**b**) or
610 lisocabtagene maraleucel, respectively (**c**). (**d**-**e**) Representative flow plots depicting gating for
611 CAR expression (top) and T-cell lineages (bottom) in CD28-costimulated (**d**) and 4-1BB-
612 costimulated (**e**) CAR T cells. (**f**, **h**) Transduction percentage as measured by meGFP
613 fluorescence among T cells from each culturing condition in CD28-costimulated (**f**, n=3) and 4-
614 1BB-costimulated (**h**, n=3) CAR T cells. (**g**, **i**) Stacked bar plot comparing CD8 vs CD4 proportions
615 in CD28-costimulated (**g**, n=3) and 4-1BB-costimulated (**i**, n=3) CAR T cells. (**j**-**m**) Cytotoxicity of
616 CD28-costimulated (**j**-**k**) and 4-1BB-costimulated (**l**-**m**) CAR T cells. (**j**, **l**) direct cytotoxicity against
617 firefly luciferase-expressing OCI-Ly8 target cells at E/T ratio of 1:1 via 6-hr bioluminescence assay
618 (n=5). (**k**, **m**) intracellular staining for granzyme B (right) and perforin (left) after 4-hr of coculture
619 with OCI-Ly8 at E/T ratio of 1:1 as measured by flow cytometry (n=3). (**n**-**o**) Concentration of
620 cytokines secreted by CD28-costimulated (**n**) and 4-1BB-costimulated (**o**) CAR T cells into the
621 supernatant after 24-hr of coculture with OCI-Ly8 at E/T ratio of 1:1 as measured by ELISA (n=5).
622 From left to right, IL-2, TNF, and IFNγ. All data are reported as mean ± standard error. Statistical
623 analysis were performed via one-way (**f**, **h**, **j**-**o**) or two-way (**g**, **i**) ANOVA with Tukey correction for
624 multiple comparisons. All panels are representative data from 3 independent donors.

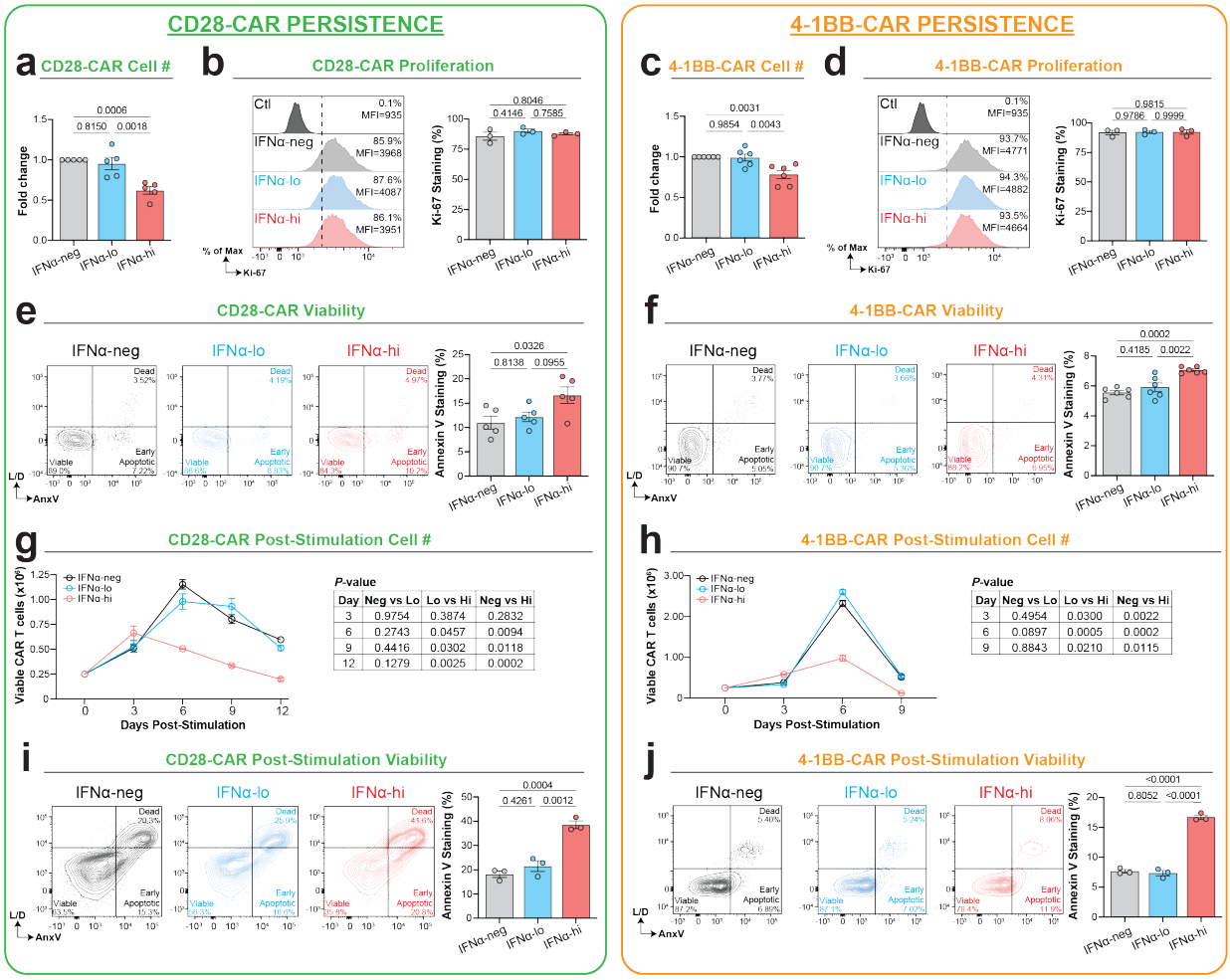
CD28-CAR PERSISTENCE
a CD28-CAR Cell #
b CD28-CAR Proliferation
e CD28-CAR Viability
g CD28-CAR Post-Stimulation Cell #
i CD28-CAR Post-Stimulation Viability
4-1BB-CAR PERSISTENCE
c 4-1BB-CAR Cell #
d 4-1BB-CAR Proliferation
f 4-1BB-CAR Viability
h 4-1BB-CAR Post-Stimulation Cell #
j 4-1BB-CAR Post-Stimulation Viability
IFNα-neg
IFNα-lo
IFNα-hi
Fold change
Ki-67 Staining (%)
Annexin V Staining (%)
Viable CAR T cells (x10⁶)
Days Post-Stimulation
P-value
Day | Neg vs Lo | Lo vs Hi | Neg vs Hi
3 | 0.9754 | 0.3874 | 0.2832
6 | 0.2743 | 0.0457 | 0.0094
9 | 0.4416 | 0.0302 | 0.0118
12 | 0.1279 | 0.0025 | 0.0002
P-value
Day | Neg vs Lo | Lo vs Hi | Neg vs Hi
3 | 0.4954 | 0.0300 | 0.0022
6 | 0.0897 | 0.0005 | 0.0002
9 | 0.8843 | 0.0210 | 0.0115

625

**Figure 3. High-strength IFN-I signaling increases apoptosis, whereas low-strength IFN-I signaling does not.**

(**a**, **c**) Relative counts of live CAR T cells from the three culturing conditions after CAR T-cell manufacturing in CD28-costimulated (**a**, n=5) and 4-1BB-costimulated (**c**, n=6) CAR T cells. Counts were normalized to the IFNα-neg condition. (**b**, **d**) Proliferation of CAR T cells from the three culturing conditions in CD28-costimulated (**b**, n=3) and 4-1BB-costimulated (**d**, n=3) CAR T cells. Left, representative flowplots depicting gating for Ki-67$^{+}$ proliferating CAR T cells at the day when IFNα was removed. Right, Ki-67$^{+}$ proliferating cell proportions among CAR T cells. Non-activated naïve T cells from human PBMCs were used as a biological control for gating. (**e**, **f**) Apoptosis of CAR T cells from the three culturing conditions after CAR T-cell manufacturing in CD28-costimulated (**a**, n=5) and 4-1BB-costimulated (**c**, n=6) CAR T cells. Left, representative flow plots depicting gating for viable, early apoptotic, and dead cells among CAR T cells. Right, staining for Annexin V positivity among live CAR T cells. (**g**, **h**) Line graphs depicting viable CAR T-cell cellularity of CD28-costimulated (**g**, n=3) and 4-1BB-costimulated (**h**, n=3) CAR T cells in vitro following coculture with OCI-Ly8 at E/T ratio of 1:5. (**i**, **j**) Apoptosis of CD28-costimulated CAR T cells (**i**, n=3) and 4-1BB-costimulated CAR T cells (**j**, n=3) from the three culturing conditions at day 6 after coculture with OCI-Ly8 cells at E/T ratio of 1:5. Left, representative flow plots depicting gating for viable, early apoptotic, and dead cells among the three culturing conditions. Right, staining for Annexin V positivity among live CAR T cells. All data are reported as mean ± standard error. Statistical analysis were performed via one-way (**a**-**f**, **i**-**j**) or two-way (**g**, **h**) ANOVA with Tukey correction for multiple comparisons. Panels **a**, **c**, **e**-**j** are representative data from 3 independent donors. Panels **b**, **d** are representative data from 2 independent donors.

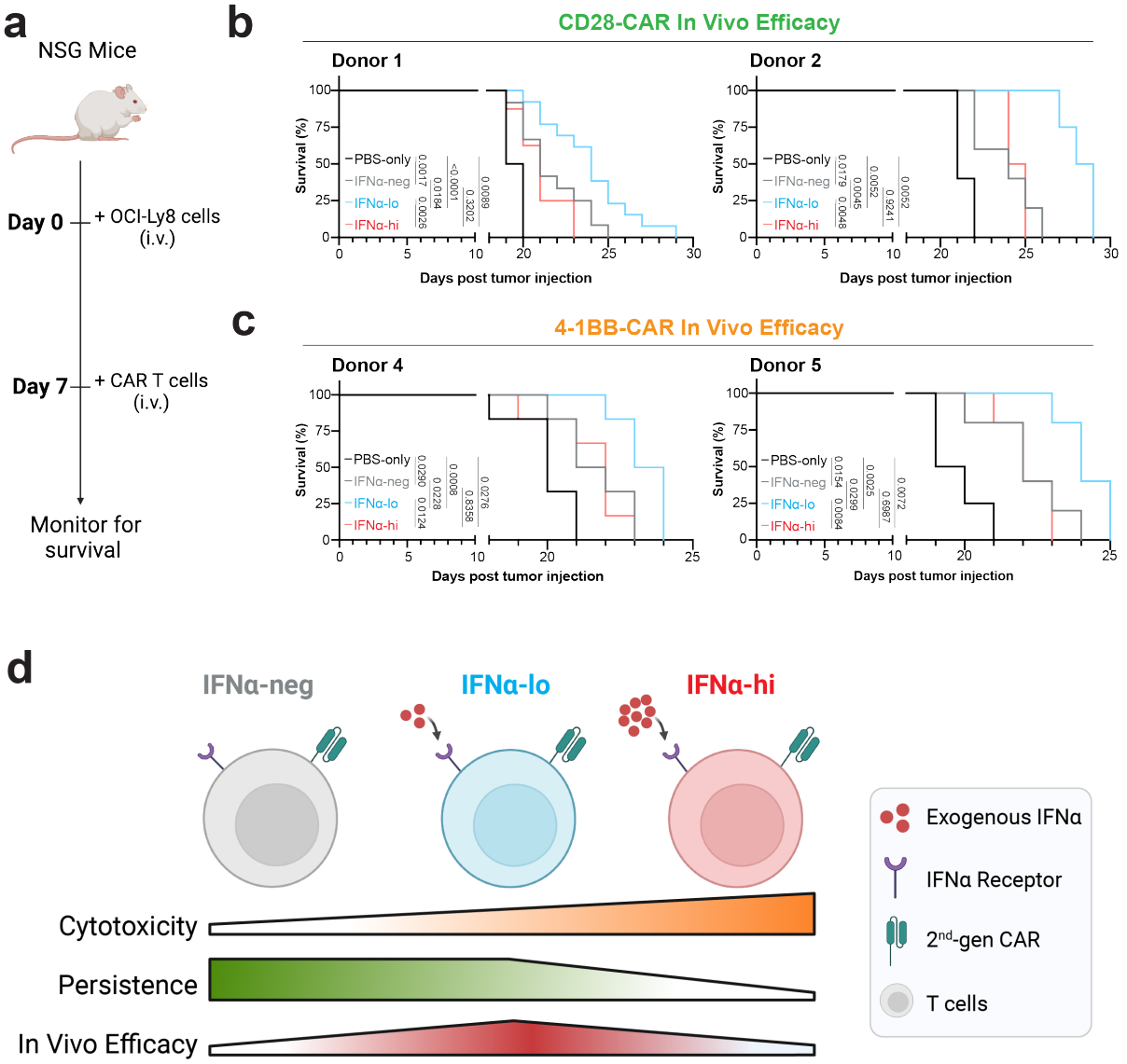


**Figure 4. Low-strength IFN-I signaling promotes CAR T-cell treatment efficacy in vivo.** (**a**) Schematic depicting timeline for NSG mouse model based on OCI-Ly8 lymphoma cell line. Seven days following OCI-Ly8 injection, mice were randomly divided into groups that were treated with either PBS or CAR T cells from the three culturing conditions. (**b**) Kaplan-Meier analysis of survival of OCI-Ly8-bearing mice treated with PBS or $5\times10^5$ CD28-costimulated CAR T cells from various culture conditions. CAR T cells were generated from donor 1 (left, n=8,12,13,8), and donor 2 (right, n=5,5,4,4). (**c**) Kaplan-Meier analysis of survival of OCI-Ly8-bearing mice treated with PBS or $5\times10^5$ (left) or $1\times10^6$ (right) 4-1BB-costimulated CAR T cells from various culture conditions. CAR T cells were generated from donor 4 (left, n=6,6,6,6), and donor 5 (right, n=4,5,5,5). (**d**) Cartoon summarizing effects of IFN-I signaling on CAR T cells at different doses. Statistical analysis were performed by log-rank (Mantel-Cox) test.